AGU PUBLICATIONS

Journal of Geophysical Research: Solid Earth

Supporting Information for

Geostatistical Inversion for Subsurface Characterization Using Stein Variational Gradient Descent with Autoencoder Neural Network: An Application to Geologic Carbon Sequestration

Mingliang Liu[1], **Dario Grana**[2] and **Tapan Mukerji**[1,3]

[1] Department of Energy Science and Engineering, Stanford University, USA.

[2] Department of Geology and Geophysics, University of Wyoming, USA.

[3] Department of Geophysics and Department of Earth & Planetary Science, Stanford University, USA.

Corresponding author: Mingliang Liu (mliu9@stanford.edu)

Contents of this file

- Text S1-S4
- Table S1-S3
- Figure S1-S4

This supporting information contains texts, tables and figures as mentioned in the main article.

Text S1. Functional derivative of Kullback-Leibler (KL) divergence

According to the invariance property of the KL divergence under parameter transformations, the following relationship holds:

$$\mathbb{D}_{KL}[q_{[\mathbf{T}]}||\pi] = \mathbb{D}_{KL}[q\,|\,|\pi_{[\mathbf{T}^{-1}]}]. \tag{S1}$$

Here, the left-hand side represents the KL divergence of the random variable before the transformation, while the right-hand side represents the KL divergence after the transformation. Hence, we have:

$$\begin{aligned}\nabla_\epsilon \mathbb{D}_{KL}[q_{[\mathbf{T}]}||\pi] &= \nabla_\epsilon \mathbb{D}_{KL}\left[q\,\middle|\,\middle|\pi_{[\mathbf{T}^{-1}]}\right] = \nabla_\epsilon \int q(\mathbf{m}) \log \frac{q(\mathbf{m})}{\pi_{[\mathbf{T}^{-1}]}(\mathbf{m})}\, d\mathbf{m} \\ &= -\nabla_\epsilon \int q(\mathbf{m}) \log \pi_{[\mathbf{T}^{-1}]}(\mathbf{m}) d\mathbf{m} = -\mathbb{E}_{\mathbf{m}\sim q}\left[\nabla_\epsilon \log \pi_{[\mathbf{T}^{-1}]}(\mathbf{m})\right] \\ &= -\mathbb{E}_{\mathbf{m}\sim q}\left[\nabla_\epsilon \log(\pi\big(\mathbf{T}(\mathbf{m})\big)\,|\mathrm{det}\,(\nabla_{\mathbf{m}}\mathbf{T}(\mathbf{m})|)\right] \\ &= -\mathbb{E}_{\mathbf{m}\sim q}\left[\nabla_\epsilon \log \pi\big(\mathbf{T}(\mathbf{m})\big) + \nabla_\epsilon \log|\mathrm{det}\,(\nabla_{\mathbf{m}}\mathbf{T}(\mathbf{m})|\right] \\ &= -\mathbb{E}_{\mathbf{m}\sim q}\left[\nabla_{\mathbf{m}} \log \pi\big(\mathbf{T}(\mathbf{m})\big)^T \nabla_\epsilon \mathbf{T}(\mathbf{m}) + \mathrm{trace}\big(\nabla_{\mathbf{m}}\mathbf{T}(\mathbf{m})^{-1}\nabla_\epsilon\nabla_{\mathbf{m}}\mathbf{T}(\mathbf{m})\big)\right].\end{aligned} \tag{S2}$$

Considering $\mathbf{T}(\mathbf{m}) = \mathbf{m} + \epsilon\boldsymbol{\phi}(\mathbf{m})$ and making a first-order approximation, we have:

$$\mathbf{T}(\mathbf{m}) \approx \mathbf{m}, \tag{S3}$$

$$\nabla_{\mathbf{m}}\mathbf{T}(\mathbf{m}) \approx \mathbf{I}, \tag{S4}$$

$$\nabla_\epsilon \mathbf{T}(\mathbf{m}) = \boldsymbol{\phi}(\mathbf{m}), \tag{S5}$$

$$\nabla_\epsilon \nabla_{\mathbf{m}} \mathbf{T}(\mathbf{m})) = \nabla_{\mathbf{m}}\boldsymbol{\phi}(\mathbf{m}). \tag{S6}$$

By substituting Equations S3 to S6 into Equation S2, we have:

$$\begin{aligned}\nabla_\epsilon \mathbb{D}_{KL}[q_{[\mathbf{T}]}||\pi] &= -\mathbb{E}_{\mathbf{m}\sim q}[\nabla_{\mathbf{m}} \log \pi(\mathbf{m})^T\, \boldsymbol{\phi}(\mathbf{m}) + \mathrm{trace}(\mathbf{I}^{-1}\nabla_{\mathbf{m}}\boldsymbol{\phi}(\mathbf{m})] \\ &= -\mathbb{E}_{\mathbf{m}\sim q}\left[\mathrm{trace}(\boldsymbol{\mathcal{A}}_\pi[\boldsymbol{\phi}_k(\mathbf{m})]\right].\end{aligned} \tag{S7}$$

where $\boldsymbol{\mathcal{A}}_\pi$ is the so-called Stein operator:

$$\boldsymbol{\mathcal{A}}_\pi[\boldsymbol{\phi}(\mathbf{m})] \triangleq \boldsymbol{\phi}(\mathbf{m})\nabla_{\mathbf{m}}\log\pi(\mathbf{m}) + \nabla_{\mathbf{m}}\boldsymbol{\phi}(\mathbf{m}). \tag{S8}$$

Text S2. Reproducing kernel Hilbert space (RKHS)

Let $\mathcal{H}$ be a Hilbert space consisting of real-valued functions $f: \mathcal{X} \to \mathbb{R}$. A function $K: \mathcal{X} \times \mathcal{X} \to \mathbb{R}$ is called a reproducing kernel of $\mathcal{H}$ if it satisfies the following conditions:

(1) $\forall x \in \mathcal{X}, K_x \coloneqq K(x,\cdot) \in \mathcal{H}$;

(2) $\forall x \in \mathcal{X}, \forall f \in \mathcal{H}, < f, K(x,\cdot) >_{\mathcal{H}} = f(x)$.

If $\mathcal{H}$ has a reproducing kernel, $\mathcal{H}$ is referred to as a reproducing kernel Hilbert space (RKHS).

Conversely, given a kernel function $K: \mathcal{X} \times \mathcal{X} \to \mathbb{R}$, a mapping $\phi: \mathcal{X} \to \mathcal{H}$ can be defined as follows:

$$x \mapsto \phi(x) \coloneqq K_x \coloneqq K(x,\cdot). \tag{S9}$$

Here, each point $x \in \mathcal{X}$ is mapped to the functional $K_x: \mathcal{X} \to \mathbb{R}$, defined by:

$$K_x(x') = K(x, x'), \forall x' \in \mathcal{X}. \tag{S10}$$

An inner product space $\mathcal{G}$ can then be constructed by taking the span of $\{\phi(x) : x \in \mathcal{X}\}$:

$$\mathcal{G} \coloneqq \mathrm{span}\{\phi(x) : x \in \mathcal{X}\}. \tag{S11}$$

The space $\mathcal{G}$ is equipped with the inner product defined as:

$$< f, g >_{\mathcal{G}} \coloneqq < \sum_i f_i K(x_i,\cdot), \sum_j g_j K(x_j,\cdot) >_{\mathcal{G}} \coloneqq \sum_{i,j} f_i g_j K(x_i, x_j). \tag{S12}$$

By taking the topological completion of $\mathcal{G}$, the resulting space $\mathcal{H} \coloneqq \bar{\mathcal{G}}$ is the RKHS associated with the given kernel function K.

Text S3. Proof of the optimal perturbation direction for SVGD (Liu and Wang, 2016)

Let $\mathcal{B} = \{f \in \mathcal{H}\colon \|f\|_{\mathcal{H}} \leq 1\}$ be the reproducing kernel Hilbert space (RKHS) associated with kernel function $K\colon \mathcal{X} \times \mathcal{X} \to \mathbb{R}$. Define $\boldsymbol{\beta}(\cdot) = \mathbb{E}_{\mathbf{m}\sim q}[K(\mathbf{m},.)\nabla_{\mathbf{m}}\log\pi(\mathbf{m}) + \nabla_{\mathbf{m}}k(\mathbf{m},.)]$ where $\boldsymbol{\beta} \in \mathcal{B}$.

For a general function $\boldsymbol{\phi} \in \mathcal{B}$, using the reproducing property introduced in Text S2, we have:

$$\begin{aligned} < \boldsymbol{\phi}, \boldsymbol{\beta} >_{\mathcal{B}} =&< \boldsymbol{\phi}, \mathbb{E}_{\mathbf{m}\sim q}[K(\mathbf{m},.)\nabla_{\mathbf{m}}\log\pi(\mathbf{m}) + \nabla_{\mathbf{m}}K(\mathbf{m},.)] >_{\mathcal{B}} \\ &= \mathbb{E}_{\mathbf{m}\sim q}[< \boldsymbol{\phi}, K(\mathbf{m},.) >_{\mathcal{B}} \nabla_{\mathbf{m}}\log\pi(\mathbf{m}) + \nabla_{\mathbf{m}} < \boldsymbol{\phi}, K(\mathbf{m},.) >_{\mathcal{B}}] \\ &= \mathbb{E}_{\mathbf{m}\sim q}[\mathrm{trace}(\boldsymbol{\phi}(\mathbf{m})\nabla_{\mathbf{m}}\log\pi(\mathbf{m}) + \nabla_{\mathbf{m}}\boldsymbol{\phi}(\mathbf{m}))] \\ &= \mathbb{E}_{\mathbf{m}\sim q}[\mathrm{trace}(\boldsymbol{\mathcal{A}}_{\pi}[\boldsymbol{\phi}(\mathbf{m})])]. \end{aligned} \tag{S13}$$

Therefore, maximizing $\mathbb{E}_{\mathbf{m}\sim q}[\mathrm{trace}(\boldsymbol{\mathcal{A}}_{\pi}[\boldsymbol{\phi}(\mathbf{m})])]$ is equivalent to maximize the inner product $< \boldsymbol{\phi}, \boldsymbol{\beta} >_{\mathcal{B}}$. Obviously, the maximum occurs when $\boldsymbol{\phi}$ is proportional to $\boldsymbol{\beta}$. Hence, the optimal perturbation direction for SVGD is:

$$\boldsymbol{\phi}^{*} \propto \boldsymbol{\beta}(\cdot) = \mathbb{E}_{\mathbf{m}\sim q}[K(\mathbf{m},.)\nabla_{\mathbf{m}}\log\pi(\mathbf{m}) + \nabla_{\mathbf{m}}K(\mathbf{m},.)]. \tag{S14}$$

Text S4. Rock physics model

The unconsolidated and consolidated sand model were developed by Dvorkin and Nur (1996) to predict the elastic properties (e.g., P- and S-wave velocities and density) of sandstones based on their porosity and other properties for different geological conditions. In both rock physics models, the matrix bulk and shear moduli (K_{mat} and μ_{mat}) are derived using the Voigt-Reuss-Hill average based on mineral fractions (e.g., clay and quartz volumes). The moduli of dry rock (K_{HM} and μ_{HM}) at the critical porosity ϕ_0 are determined through the Hertz-Mindlin equations (Mindlin, 1949):

$$K_{\mathrm{HM}} = \sqrt[3]{\frac{P_e[n_c(1-\phi_0)\mu_{\mathrm{mat}}]^2}{18[\pi(1-\nu_{\mathrm{mat}})]^2}}, \tag{S15}$$

$$\mu_{\mathrm{HM}} = \frac{5-4\nu_{\mathrm{mat}}}{5(2-\nu_{\mathrm{mat}})}\sqrt[3]{\frac{3P_e[n_c(1-\phi_0)\mu_{\mathrm{mat}}]^2}{2[\pi(1-\nu_{\mathrm{mat}})]^2}}, \tag{S16}$$

where P_e is the effective pressure, ν_{mat} is the grain Poisson's ratio and n_c is the coordination number, which refers to the average number of grain contacts.

In the unconsolidated sand model, the dry rock moduli (K_{dry} and μ_{dry}) for porosity within the range [0, ϕ_0] are obtained by interpolating two end members: the matrix moduli and dry rock moduli at critical porosity, using the modified Hashin-Shtrikman lower bounds:

$$K_{\mathrm{dry}} = \left(\frac{\frac{\phi}{\phi_0}}{K_{\mathrm{HM}}+\frac{4}{3}\mu_{\mathrm{HM}}} + \frac{1-\frac{\phi}{\phi_0}}{K_{\mathrm{mat}}+\frac{4}{3}\mu_{\mathrm{HM}}}\right)^{-1} - \frac{4}{3}\mu_{\mathrm{HM}}, \tag{S17}$$

$$\mu_{\mathrm{dry}} = \left(\frac{\frac{\phi}{\phi_0}}{\mu_{\mathrm{HM}}+\frac{1}{6}\xi\mu_{\mathrm{HM}}} + \frac{1-\frac{\phi}{\phi_0}}{\mu_{\mathrm{mat}}+\frac{1}{6}\xi\mu_{\mathrm{HM}}}\right)^{-1} - \frac{1}{6}\xi\mu_{\mathrm{HM}}, \tag{S18}$$

with

$$\xi = \frac{9K_{\mathrm{HM}} + 8\mu_{\mathrm{HM}}}{K_{\mathrm{HM}} + 2\mu_{\mathrm{HM}}}. \tag{S19}$$

Similarly, the consolidated sand model uses the modified Hashin-Shtrikman upper bounds to interpolate the elastic moduli values for porosities ranging from 0 to the critical porosity ϕ_0:

$$K_{\mathrm{dry}} = \left(\frac{\frac{\phi}{\phi_0}}{K_{\mathrm{HM}}+\frac{4}{3}\mu_{\mathrm{mat}}} + \frac{1-\frac{\phi}{\phi_0}}{K_{\mathrm{mat}}+\frac{4}{3}\mu_{\mathrm{mat}}}\right)^{-1} - \frac{4}{3}\mu_{\mathrm{mat}}, \tag{S20}$$

$$\mu_{\mathrm{dry}} = \left(\frac{\frac{\phi}{\phi_0}}{\mu_{\mathrm{HM}}+\frac{1}{6}\xi\mu_{\mathrm{mat}}} + \frac{1-\frac{\phi}{\phi_0}}{\mu_{\mathrm{mat}}+\frac{1}{6}\xi\mu_{\mathrm{mat}}}\right)^{-1} - \frac{1}{6}\xi\mu_{\mathrm{mat}}, \tag{S21}$$

With

$$\xi = \frac{9K_{\mathrm{mat}} + 8\mu_{\mathrm{mat}}}{K_{\mathrm{mat}} + 2\mu_{\mathrm{mat}}}. \tag{S22}$$

For rocks saturated with fluid, Gassmann's equations (Gassmann, 1951) are used to compute the bulk shear moduli (K_{sat} and μ_{sat})

$$K_{\mathrm{sat}} = K_{\mathrm{dry}} + \frac{\left(1-\frac{K_{\mathrm{dry}}}{K_{\mathrm{mat}}}\right)^2}{\frac{\phi}{K_{\mathrm{fl}}}+\frac{1-\phi}{K_{\mathrm{mat}}}-\frac{K_{\mathrm{dry}}}{K_{\mathrm{mat}}^2}}, \tag{S23}$$

$$\mu_{\mathrm{sat}} = \mu_{\mathrm{dry}}. \tag{S24}$$

where K_{fl} is the bulk modulus of the fluid phase calculated from the brine water and supercritical CO_2 saturations (s_{bw} and s_{CO2}) and their corresponding bulk moduli (K_{bw} and K_{CO2}). We assume that the fluid components are homogeneously mixed and the effective bulk modulus by K_{fl} is computed using Wood's averaging method (Mavko et al., 2020):

$$K_{\mathrm{fl}} = \frac{1}{\frac{s_{\mathrm{bw}}}{K_{\mathrm{bw}}} + \frac{s_{\mathrm{CO2}}}{K_{\mathrm{CO2}}}}. \tag{S25}$$

For reservoirs with uneven fluid distribution, like in-situ patchy saturation, it is recommended to use Voigt or Brie's equations (Mavko et al., 2020) for the fluid mixture.

Finally, the P- and S-wave velocities can be computed from the moduli by definition as

$$V_p = \sqrt{\frac{K_{\mathrm{sat}}+\frac{4}{3}\mu_{\mathrm{sat}}}{\rho_{\mathrm{sat}}}}, \tag{S26}$$

$$V_s = \sqrt{\frac{\mu_{\mathrm{sat}}}{\rho_{\mathrm{sat}}}}, \tag{S27}$$

where ρ_{sat} is the density of the saturated rock which is weighted average of the matrix density ρ_{mat} and fluid density ρ_{fl}

$$\rho_{\mathrm{sat}} = (1-\phi)\rho_{\mathrm{mat}} + \phi\rho_{\mathrm{fl}}. \tag{S28}$$

The effective bulk modulus of the matrix ρ_{mat} and fluid mixture ρ_{fl} are provided by the Voigt average as

$$\rho_{\mathrm{mat}} = (1-v_{\mathrm{cl}})\rho_{\mathrm{qtz}} + v_{\mathrm{cl}}\rho_{\mathrm{cl}}, \tag{S29}$$

$$\rho_{\mathrm{fl}} = (1 - s_{\mathrm{CO2}})\rho_{\mathrm{bw}} + s_{\mathrm{CO2}}\rho_{\mathrm{CO2}}, \tag{S30}$$

where v_{cl} and s_{CO2} are the volumetric fractions of clay and CO_2 saturation, respectively; and ρ_{qtz}, ρ_{cl}, ρ_{bw} and ρ_{CO2} are the density of quartz, clay, brine water and supercritical CO_2, respectively.

Text S1. Rock physics parameters associated with the unconsolidated sand model in Example 2.

Parameter	**Value**
Bulk modulus of quartz	36.6 GPa
Shear modulus of quartz	44.0 GPa
Density of quartz	2.65 g/cm^3
Bulk modulus of clay	21.0 GPa
Shear modulus of clay	9.0 GPa
Density of clay	2.5 g/cm^3
Bulk modulus of brine	3.06 GPa
Density of brine	1.08 g/cm^3
Effective pressure	0.02 GPa
Critical porosity	0.4
Coordination number	7

Table S2. Architecture of the autoencoder neural network in Example 2 (N_m represents the number of different reservoir properties).

Layer	Output size
1. Input	N_mx101
2. Conv1D + Upsample	4x51
3. Conv1D + Upsample	8x26
4. Conv1D + Upsample	16x13
5. Conv1D + Upsample	32x7
6. Conv1D + Upsample	32x4
7. Tanh	32x4
8. Conv1D + Downsample	32x7
9. Conv1D + Downsample	16x13
10. Conv1D + Downsample	8x26
11. Conv1D + Downsample	4x51
12. Conv1D + Downsample	N_mx101
13. CustomLinearActivation*	N_mx101

* The customized activation function is linear between 0 and 1, assigning a value of 0 if the output is less than 0 and a value of 1 if the output exceeds 1.

Table S3. Architecture of the autoencoder neural network in Example 3 (N_m represents the number of different reservoir properties).

Layer	**Output size**
14. Input	N_mx201
15. Conv1D + Upsample	4x101
16. Conv1D + Upsample	8x51
17. Conv1D + Upsample	16x26
18. Conv1D + Upsample	32x13
19. Conv1D + Upsample	32x7
20. Tanh	32x7
21. Conv1D + Downsample	32x13
22. Conv1D + Downsample	16x26
23. Conv1D + Downsample	8x51
24. Conv1D + Downsample	4x101
25. Conv1D + Downsample	N_mx201
26. CustomLinearActivation*	N_mx201

* The customized activation function is linear between 0 and 1, assigning a value of 0 if the output is less than 0 and a value of 1 if the output exceeds 1.

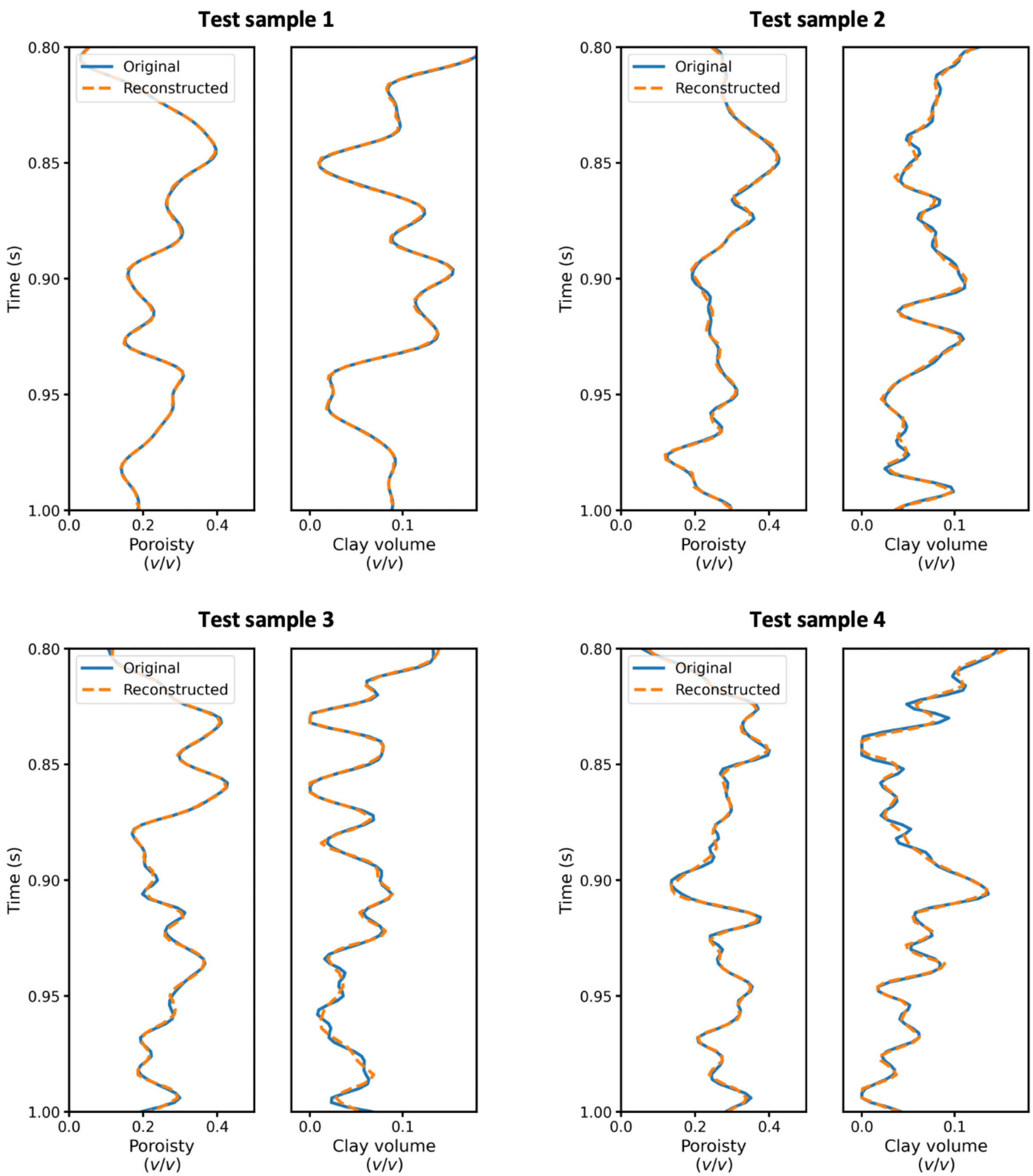

Figure S1. Comparison between the original reservoir models in the test set of Example 2 and their corresponding reconstructions by the trained autoencoder.

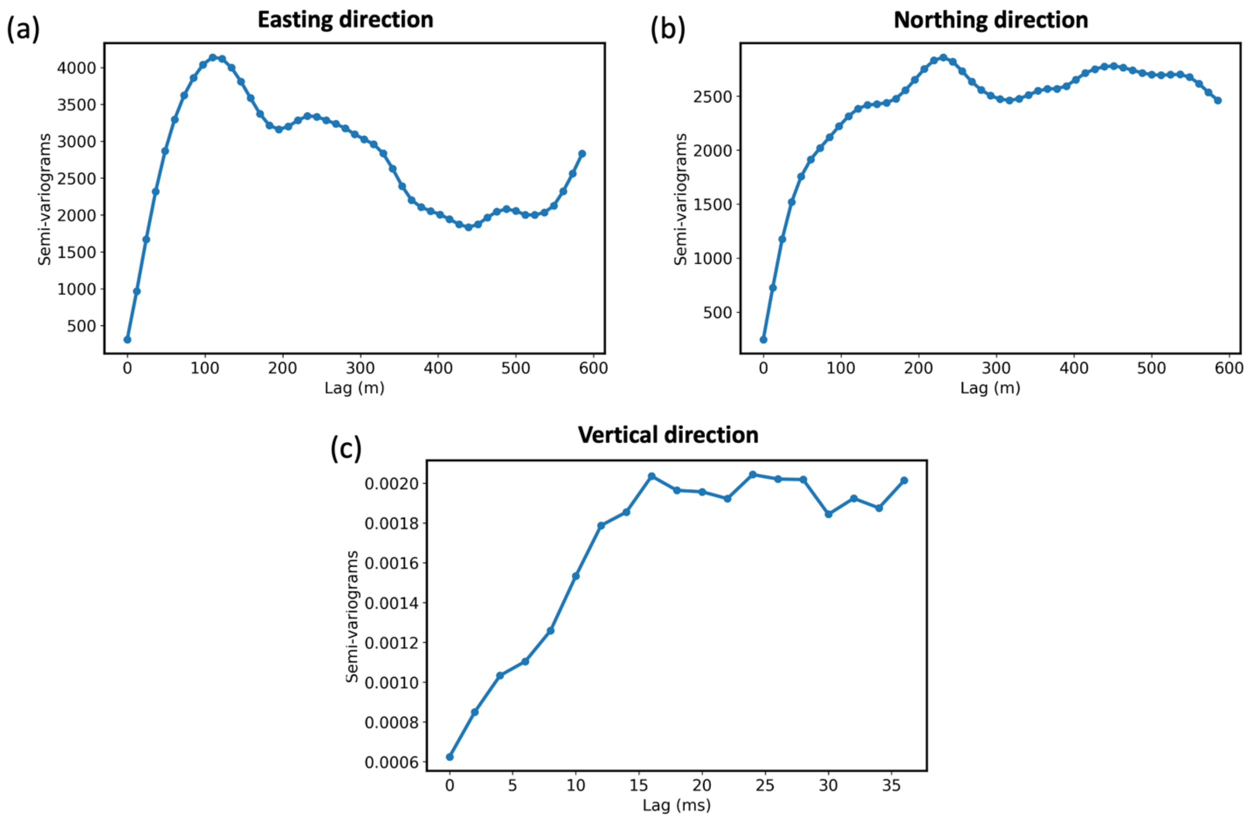

Figure S2. Experimental variograms of the IBDP case: (a) easting direction; (b) northing direction; (c) vertical direction.

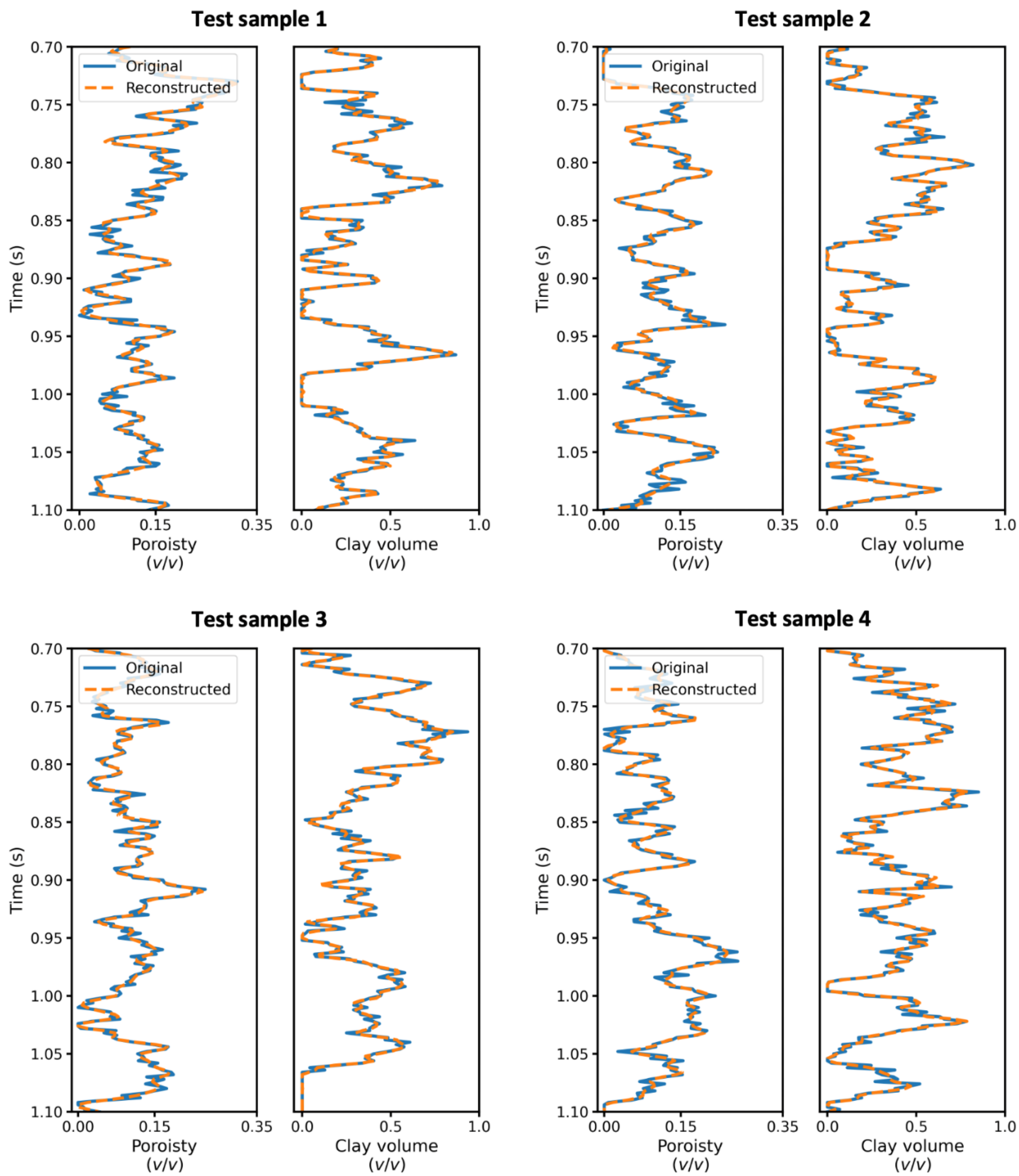

Figure S3. Comparison between the original reservoir models in the test set of the IBDP case and their corresponding reconstructions by the trained autoencoder.

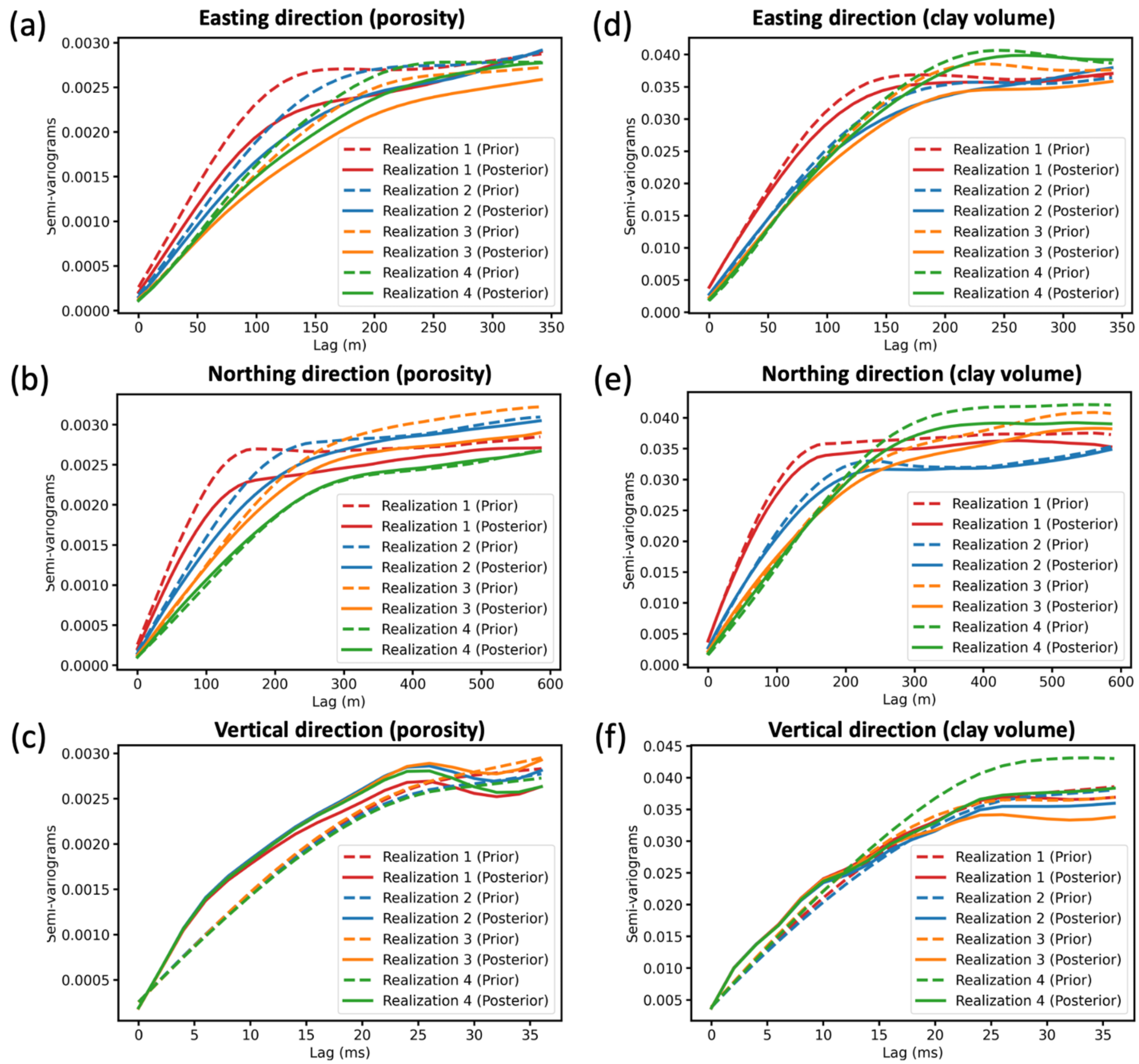

Figure S4. Experimental variograms for the prior and posterior reservoir models in the IBDP case: (a)-(c) variograms of porosity in easting, northing and vertical direction, respectively; (d)-(f) variograms of clay volume in easting, northing and vertical direction, respectively.

References

- Dvorkin, J., & Nur, A. (1996). Elasticity of high-porosity sandstones: Theory for two North Sea data sets. *Geophysics, 61*(5), pp.1363-1370.
- Gassmann, F. (1951). Elastic waves through a packing of spheres. *Geophysics, 16*(4), pp.673-685.
- Liu, Q. and Wang, D. (2016). Stein variational gradient descent: A general purpose Bayesian inference algorithm. *Advances in neural information processing systems*, 29.
- Mavko, G., Mukerji, T. and Dvorkin, J. (2020). The rock physics handbook. *Cambridge University Press*.
- Mindlin, R.D. (1949). Compliance of elastic bodies in contact. *Journal of Applied Mechanics, ASME, 16*(3), 259–268.